


CD146 expression regulates osteochondrogenic differentiation of human adipose-derived stem cells

Maria Giovanna Scioli¹ | Gabriele Storti² | Alessandra Bielli¹ |
Massimo Sanchez³ | Manuel Scimeca⁴ | Jeffrey M. Gimble⁵ | Valerio Cervelli² |
Augusto Orlandi^{1,6} 

¹Anatomic Pathology, Department of Biomedicine and Prevention, University of Rome Tor Vergata, Rome, Italy

²Plastic and Reconstructive Surgery, Department of Surgical Sciences, University of Rome Tor Vergata, Rome, Italy

³Major Equipments and Core Facilities, Istituto Superiore di Sanità, Rome, Italy

⁴Anatomic Pathology, Department of Experimental Medicine, University of Rome Tor Vergata, Rome, Italy

⁵Department of Pharmacology, Center for Stem Cell Research and Regenerative Medicine, Tulane University, New Orleans, Louisiana, USA

⁶Department of Biomedical Sciences, Catholic University Our Lady of Good Counsel, Tirana, Albania

Correspondence

Augusto Orlandi, Anatomic Pathology, Department of Biomedicine and Prevention, University of Rome Tor Vergata, Via Montpellier, 00133 Rome, Italy.
Email: orlandi@uniroma2.it

Abstract

Tissue engineering aims to develop innovative approaches to repair tissue defects. The use of adipose-derived stem cells (ASCs) in tissue regeneration was extensively investigated for osteochondrogenesis. Among the ASC population, ASCs expressing the CD146 were demonstrated to be multipotent and considered as perivascular stem cells, although the functional role of CD146 expression in these cells remains unclear. Herein, we investigated the influence of CD146 expression on osteochondrogenic differentiation of ASCs. Our results showed that, in two-dimensional culture systems, sorted CD146⁺ ASCs proliferated less and displayed higher adipogenic and chondrogenic potential than CD146⁻ ASCs. The latter demonstrated a higher osteogenic capacity. Besides this, CD146⁺ ASCs in three-dimensional Matrigel/endothelial growth medium (EGM) cultures showed the highest angiogenic capability. When cultured in three-dimensional collagen scaffolds, CD146⁺ ASCs showed a spontaneous chondrogenic differentiation, further enhanced by the EGM medium's addition. Finally, CD146⁻ ASCs seeded on hexafluoroisopropanol silk scaffolds displayed a greater spontaneous osteogenetic capacity. Altogether, these findings demonstrated a functional and relevant influence of CD146 expression in ASC properties and osteochondrogenic commitment. Exploiting the combination of specific differentiation properties of ASC subpopulations and appropriate culture systems could represent a promising strategy to improve the efficacy of new regenerative therapies.

KEYWORDS

CD146, cell sorting, differentiation, human adipose-derived stem cells, tissue regeneration

1 | INTRODUCTION

Interest in the study of adult stem/progenitor cells for therapeutic applications has grown in recent decades (Liu et al., 2020). Numerous sources of adult stem/progenitor cells have been reported, and each

tissue-resident stem/progenitor population displays different functions and potentialities (Liu et al., 2020). Human bone marrow and adipose tissue have been suggested as potential stem cell sources for tissue repairing therapies (Cho et al., 2005; Kang et al., 2005; Mauney et al., 2007).

Maria Giovanna Scioli and Gabriele Storti contributed equally to this study.

Adipose tissue contains many mesenchymal stem/progenitor cells, isolated through collagenase digestion as a part of the stromal vascular fraction (Gimble et al., 2007). The latter is a heterogeneous mixture of cells in which we find the so-called adipose-derived stem/stromal/progenitor cells (ASCs; Cervelli et al., 2009; Matsumoto et al., 2006; Zuk et al., 2002). Multipotential differentiation properties of ASCs represent an advantage for therapeutic application; nevertheless, uncontrolled differentiation toward other cell types may entail possible issues in regard to tissue functioning. Several studies have been performed to isolate ASC subpopulations, optimize their use, and better address differentiation. Traktuev et al. (2008) first demonstrated the perivascular localization of ASCs, while later on, other authors described the existence of CD146⁻ adventitial cells and CD146⁺ (or MUC18⁺) pericytes within the ASC population (Corselli et al., 2012; Zimmerlin et al., 2012). Both subpopulations of ASCs were demonstrated to be multipotent and were renamed human perivascular stem cell subpopulations (hPSCs; James et al., 2012). Different authors proposed the hPSCs as mesenchymal progenitor cells with a more pronounced stem phenotype (Corselli et al., 2010; Crisan et al., 2008; James et al., 2012; Zannettino et al., 2008). Previous studies have highlighted that the whole ASC population and the perivascular CD146⁺ cells share similar features, suggesting these cells as the progenitors among the ASCs (Crisan et al., 2008; Zimmerlin et al., 2012, 2010). Nonetheless, other authors advocated the stem role for the CD146⁻ cells, underlying critical phenotypic differences between ASCs and the CD146⁺ population (Corselli et al., 2010, 2012; Hardy et al., 2017; Zannettino et al., 2008). It has been reported that there exists the central role of CD146 in the development of the vascular system of human placental extravillous trophoblast (Kaspi et al., 2013), in angiogenesis and stem cell phenotype maintenance of human endothelial progenitor cells (Essaadi et al., 2018) and in vascular repair (Joshkon et al., 2020). However, the functional implications of CD146 expression in ASCs remain unclear. In this study, we sorted CD146⁺ and CD146⁻ cell subpopulations from human ASCs and compared their osteochondral potential through the use of two different three-dimensional (3D) culture systems, particularly collagen gel and hexafluoroisopropanol (HFIP) silk scaffold. We documented how CD146 expression, combined with specific culture systems, greatly influenced the osteochondral differentiation of ASCs.

2 | MATERIALS AND METHODS

2.1 | Ethics statement

Anonymized small samples of human cartilage from nondiagnostic surgical samples were taken under the patients' written informed consent and in accordance with the guidelines of the Declaration of Helsinki and the local Ethics Committee on Human Research of the University of Rome Tor Vergata.

2.2 | ASC sorting and culture

ASCs were isolated from subcutaneous adipose tissue obtained through liposuction procedures and cultured, as reported (Cervelli et al., 2009). ASC immunophenotype was confirmed by flow cytometry at passage 0 (Scioli et al., 2018). The same passage was used to sort CD146^{+/−} ASCs (for details, see Supporting Information Materials and Methods). After sorting, cells were seeded at a density of 2500 cells/cm² and allowed to reach a confluency of 80% (P1) in the basal medium. Cells were then passaged by trypsin (0.05%) digestion and reseeded (P2) in the basal medium. All experiments were performed using pooled (*n* = 3) sorted ASCs at passage 3 after rechecking the CD146 expression by flow cytometry. In some experimental conditions, ASCs were cultured with an endothelial growth medium (EGM™ BulletKit; Lonza). The medium was changed every 3 days.

2.3 | Assessment of adipogenic, osteogenic, and chondrogenic differentiation in a 2D-culture system

The adipogenic, osteogenic, and chondrogenic differentiation capability of unsorted ASCs and CD146⁺ and CD146⁻ subpopulations were assessed on a plastic dish on confluent cells at passage 3. Adipogenic differentiation was induced, and intracytoplasmic lipid accumulation was assessed by Oil Red O staining and quantified as previously described (Cervelli et al., 2009, 2012). Osteogenic differentiation was induced as reported (Cervelli et al., 2009), and mineralization as intracellular calcium deposits was assessed by Alizarin Red S staining (Mitchell et al., 2006). Intracellular calcium accumulation was evaluated to quantify mineralization after the Alizarin Red staining by elution with 10% (wt/vol) cetylpyridinium chloride (Sigma-Aldrich) for 1 h, and then the absorbance measured at 570 nm (Binulal et al., 2010). For chondrogenic differentiation, 2 × 10⁵ cells were placed into polypropylene tubes containing 1 ml of control medium, as reported (Merceron et al., 2012). After differentiation, pellets were retrieved, fixed in 4% paraformaldehyde for histology (Alcian Blue staining), or frozen at −80°C for 1,9-dimethylmethylene blue (DMMB) assay (Scioli et al., 2017). Stainings were photographed by an E600 Eclipse microscope (with a digital camera Dxm1200F; Nikon) using an ACT-1 software (Nikon). Reported values represent the mean of three independent experiments performed in triplicate.

2.4 | Growth curve

CD146⁺ and CD146⁻ ASCs (and unsorted cells) were seeded at a density of 2500 cells/cm² in 24-well plates and incubated for 24 h in basal medium. After 24 h of starvation (with 0.1% fetal bovine serum), the cells were placed back in the basal medium. The medium was changed every 2 days. After 2, 4, and 6 days of culture, the cells were digested with 0.25% trypsin solution and then counted, with a trypan-blue exclusion, using a hemocytometer. Reported results

were the mean value of three independent experiments performed in triplicate.

2.5 | Tube formation assay in Matrigel

A tube formation assay was performed in eight multiwell chamber slides (BD Biosciences) with a minimal volume of Matrigel basement membrane matrix, which allowed the formation of both tubules and a vascular network. Before the assay, cells were grown for 72 h in basal or endothelial growth medium (EGM), specific for pericytes/endothelial cells. Then, the cells were seeded on Matrigel at a density of 2×10^5 cells/100 μ l for a further 24 h. In other experiments, human umbilical vein endothelial cells (HUVECs; Innoprot) were grown for 72 h in a basal or conditioned medium, derived from ASCs that had been cultured for 3 days in basal medium, and they were then seeded on Matrigel at a density of 2×10^5 cells/100 μ l for a further 24 h. Ten fields at $\times 40$ (original magnification) were randomly selected, photographed, and tube length quantified using Image Viewer software (BioImagene Inc., Roche Diagnostics). At the end of the experiment, cells were fixed in 4% paraformaldehyde and tested for the expression of the endothelial marker von Willebrand factor (vWF) through immunofluorescence (see below). Reported results were the mean value of three independent experiments performed in triplicate.

2.6 | Scratch test

HUVECs were cultured until confluence, then monolayers were scratched, and EGM, unconditioned or conditioned basal medium from ASCs added to monolayers to test their wound-healing properties (for details, see Supporting Information Materials and Methods). Results are the mean of three independent experiments performed in triplicate.

2.7 | Immunofluorescence

After the tube formation assay, ASCs were fixed in 4% paraformaldehyde for 5 min at 4°C and then incubated with mouse anti-vWF polyclonal antibody (Dako Cytomation) for 1 h at room temperature. A specific fluorescent secondary antibody (PE goat anti-rabbit immunoglobulin G; Nordic-MUBio) was added, and Hoechst was used for nuclear staining (Scioli et al., 2014). Images were acquired, and tube length quantified as reported above.

2.8 | Collagen gel cell-populated scaffolds

A solution of rat tail collagen type I (BD Bioscience) was used to prepare a 3D scaffold at a final concentration of 1.8 mg/ml, as reported (Scioli et al., 2017) with minor modification. Briefly, ASCs at a density of 2×10^5 cells/350 μ l/well (24-well plates) were seeded into collagen gel scaffolds and maintained in basal medium or EGM for 15

days. The contraction was measured by calculating the gel diameter (Scioli et al., 2017). Results are the mean of three independent experiments performed in triplicate. After measurements, collagen gels were either frozen at -80°C for DMMB assays and biomolecular studies or fixed into 4% paraformaldehyde for histochemical/immunohistochemical stainings.

2.9 | HFIP silk cell-populated scaffolds

HFIP silk scaffolds, previously reported to sustain ASC viability and differentiation (Frazier et al., 2016; Mauney et al., 2007), were kindly provided by Prof. Jeffrey M. Gimble (Tulane University). After a prewetting overnight at $+4^\circ\text{C}$ in basal medium, HFIP silk scaffolds were seeded with ASCs at passage 3. To this aim, cells were loaded, via pipetting in two aliquots of 50 μ l, each containing 2.5×10^5 cells, onto opposite faces of a cylindrical HFIP silk scaffold (Frazier et al., 2016). Then scaffolds were transferred to a humidified 37°C , 5% CO_2 incubator and rotated every 15 min over a 2 h period, followed by the addition of 5 ml of basal medium or EGM for 15 days. Scaffolds were fixed in 4% paraformaldehyde for histochemical/immunohistochemical analysis or frozen at -80°C for DMMB assays. All experiments were performed in triplicate, each being repeated at least three times.

2.10 | Histochemical and immunohistochemical analysis

Collagen gels and HFIP silk scaffolds were fixed in 4% paraformaldehyde for 20 min and embedded in paraffin. Then, 44- μ m thick sections were either stained with hematoxylin & eosin (H&E) or used for histochemical (Alcian Blue and Alizarin Red) or immunohistochemical stainings (Scioli et al., 2017). For the immunohistochemistry, 4- μ m thick sections were deparaffinized, rehydrated and, after antigen retrieval and nonspecific peroxidase blocking, incubated with rabbit polyclonal anti-CD31 (1:300 1 h at room temperature [RT]; Abcam) and α -SMA (1:100 1 h at RT; Dako), as reported (Scioli et al., 2017).

2.11 | Reverse transcriptase and real-time polymerase chain reaction

After total RNA extraction, reverse-transcriptase or real-time polymerase chain reaction (Stasi et al., 2010) were performed for human osteocalcin (OCN), alkaline phosphatase (ALP), aggrecan (ACAN), collagen type II (COL2A1), collagen type X (COL10A1), matrix metalloproteinase 13 (MMP13), and CD31 (Table 1). Human glyceraldehyde-3 phosphate dehydrogenase was used as a house-keeping gene, and results were reported as a normalized expression. Results are the mean of three independent experiments performed in triplicate.

TABLE 1 Primers used for RT-PCR and real-time PCR

Gene	Primer sequence	Accession number	Temperature of annealing (°C)
ALP	Sense 5'-ACGTGGCTAAGAATGTCATC-3'	NM_000478.4	58
	Antisense 5'-CTGGTAGGCGATGTCCTT-3'		
OCN	Sense 5'-CAAAGGTGCAGCCTTTGTGTC-3'	NM_199173.4	62
	Antisense 5'-TCACAGTCCGGATTGAGCTCA-3'		
Aggrecan	Sense 5'-TACTCTGGGTTTTTCGTGACTC-3'	NM_001135.3	56
	Antisense 5'-CGATGCCTTTCACCACGACTT-3'		
COL2A1	Sense 5'-GCCTGGTGCATGGGTTT-3'	NM_000088.3	56
	Antisense 5'-GTCCCTTTCACCAGCTTTG-3'		
COL10A1	Sense: 5'-GCACGCAGAATCCATCTGAGAATA-3'	NM_000493.3	60
	Antisense: 5'-GACCAGGAGTACCTTGCTCTC-3'		
MMP13	Sense: 5'-ATGCATCCAGGGTCCTGGC-3'	NM_001135.3	60
	Antisense: 5'-TGCTGCATTCTCCTCAGGA-3'		
CD31	Sense 5'-GCCAGTTGAGAACTCTGC-3'	NM_000442.5	58
	Antisense 5'-TGGGTTGTACCTTCCAGGAG-3'		
GAPDH	Sense 5'-ACGGATTGGTCGTATTGG-3'	NM_002046	58
	Antisense 5'-GATTTGGAGGGATCTCGC-3'		

Abbreviation: RT-PCR, reverse transcription-polymerase chain reaction.

2.12 | Transmission electron microscopy

For transmission electron microscopy (TEM), 1-mm thick collagen gel samples were fixed and processed (Cervelli et al., 2012). Ultrathin sections were counterstained with uranyl acetate and lead citrate and photographed using a Hitachi 7100 transmission electron microscope. Mouse articular cartilage was used as the positive control.

2.13 | Scanning electron microscopy

At the end of the experimental phase, scaffolds were fixed in Karnovsky solution for 24 h. After washing with 0.1 M phosphate buffer, the sample was dehydrated by a series of incubations in 30, 50, and 70% (vol/vol) ethanol. Dehydration was carried on through incubation steps in 95% (vol/vol) ethanol, absolute ethanol, and acetone. Critical point drying (Agar Scientific, Elektron Technology UK Ltd.) with supercritical CO₂ was then performed to prevent cell deformation. A scanning electron microscope (SEM) LEO 1450VP (Carl Zeiss Meditec) was employed to acquire images.

2.14 | Energy dispersive X-ray microanalysis

Energy dispersive X-ray (EDX) microanalysis was performed for chemical analysis (Scimeca et al., 2018). Spectra were collected by an SEM LEO 1450VP at an acceleration voltage of 5 KeV, employing an area scan mode (640 × 640 μm sampling area), 300 s acquisition

time, and 32%–37% detector dead time. Microanalysis was performed under a nonstandard mode using atomic number-absorption-fluorescence correction (ZAF) methods, which employ the Inca Energy software (Oxford Instruments Ltd.; Si(Li) detector, atmospheric thin window, resolution 133 eV for MnK α at 10,000 counts).

2.15 | Statistical analysis

Results were expressed as the mean \pm standard error of the mean and analyzed by Student's *t*-test. Differences were considered statistically significant for $p < .05$.

3 | RESULTS

3.1 | Characterization of CD146⁺ and CD146⁻ ASC subpopulations

Sorted CD146⁻ ASCs cultured on plastic dishes in the presence of basal medium displayed a somehow more pronounced spindle-shaped morphology than CD146⁺ ASCs (Figure 1a). Moreover, the growth curve showed an increased proliferation rate of the CD146⁻, compared with the CD146⁺ and the unsorted ASCs (Figure 1b; $p < .05$ and $p < .001$ at 4 and 6 days, respectively); furthermore, CD146⁺ ASCs grew more slowly than unsorted ASCs ($p < .01$ at 4 and 6 days). Assessment for adipogenic, osteogenic, and chondrogenic differentiation revealed a higher adipogenic and an

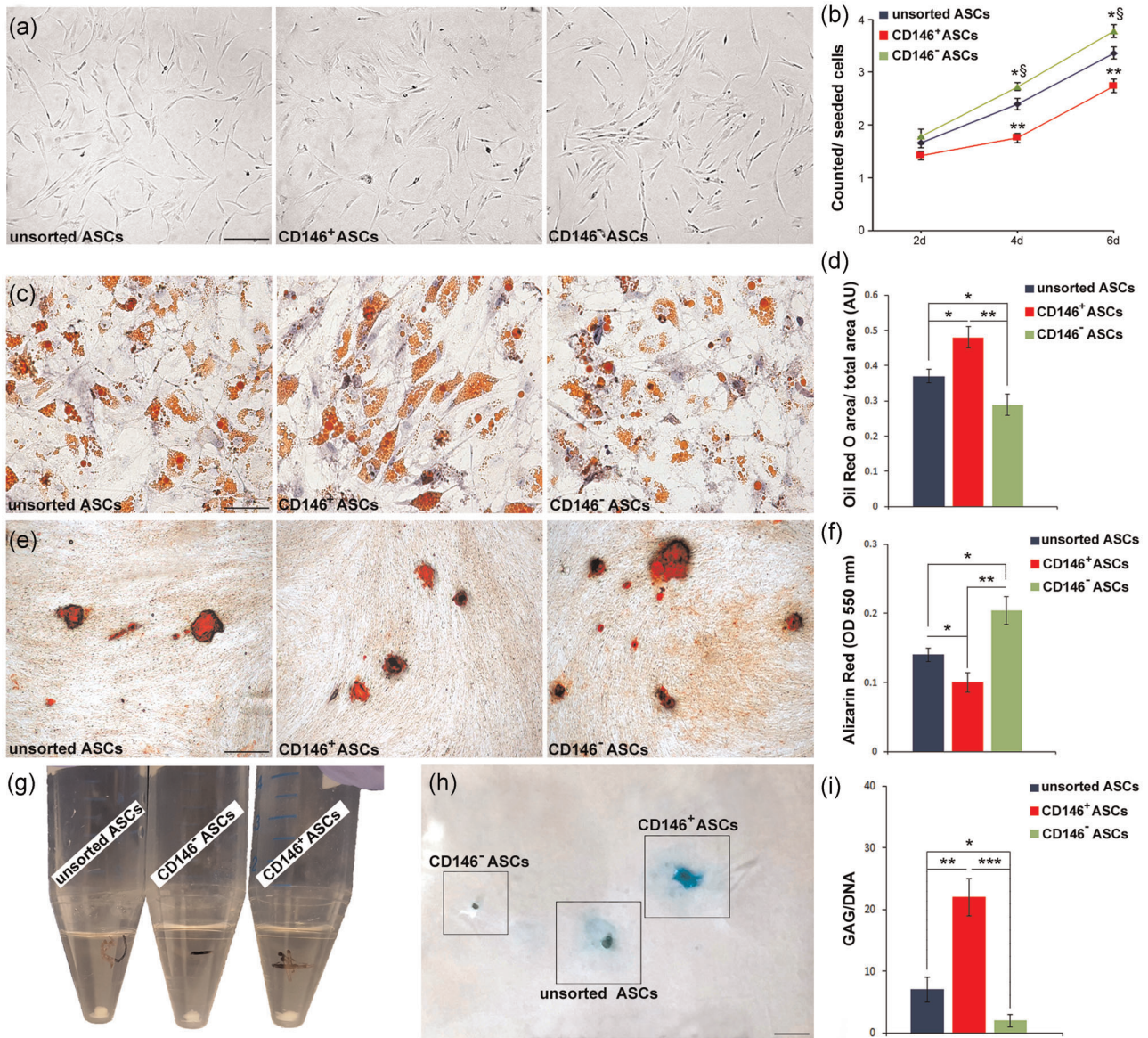


FIGURE 1 Human CD146⁺ and CD146⁻ ASCs display distinct proliferative and differentiation properties. (a) Phase-contrast microphotograph showing the typical spindle-shaped morphology of unsorted, CD146⁺, and CD146⁻-sorted ASCs, at passage 3, seeded in a plastic dish and cultured in DMEM + 10% FBS (Scale bar = 100 μ m). (b) Growth curves show unsorted CD146⁺ and CD146⁻ ASC proliferation rate at passage 3. t-Test: * $p < .05$ and ** $p < .01$ vs. unsorted ASCs; $^{\S}p < .001$, CD146⁻ ASCs vs. CD146⁺ ASCs. (c,d) Oil Red O staining and morphometric evaluation of unsorted, CD146⁺ and CD146⁻ ASCs at passage 3, seeded in a plastic dish and cultured in a standard adipogenic differentiation medium for 15 days (Scale bar = 50 μ m). (e,f) Alizarin Red staining and calcium deposit assessment after osteogenic differentiation using a standard protocol for 15 days (scale bar = 250 μ m). Images of cultured cell pellets (g), Alcian Blue staining (h), and GAG measurement after chondrogenic differentiation (i) using a standard protocol for 15 days. Reported values represent the mean \pm SEM of three independent experiments. ASC, adipose-derived stem cell; DMEM, Dulbecco's modified Eagle's medium; FBS, fetal bovine serum; GAG, glycosaminoglycan. t-Test: * $p < .05$, ** $p < .01$ and *** $p < .001$

even stronger chondrogenic differentiation capability of CD146⁺ compared to CD146⁻ (Figure 1c-i; $p < .01$ and $p < .001$, respectively) and unsorted ASCs ($p < .05$ and $p < .01$, respectively). Concerning osteogenic differentiation, CD146⁻ showed a greater potential than CD146⁺ and unsorted ASCs ($p < .01$ and $p < .05$, respectively). Finally, sorted CD146⁺ and CD146⁻ ASC

subpopulations were tested for stromal cell markers expression. No difference was found between the two subpopulations in terms of the percentage of CD90⁺ and CD44⁺ cells (Figure S1a,b). Altogether, these findings demonstrated differences among ASCs in terms of differentiation properties, according to their CD146 expression in bidimensional cultures.

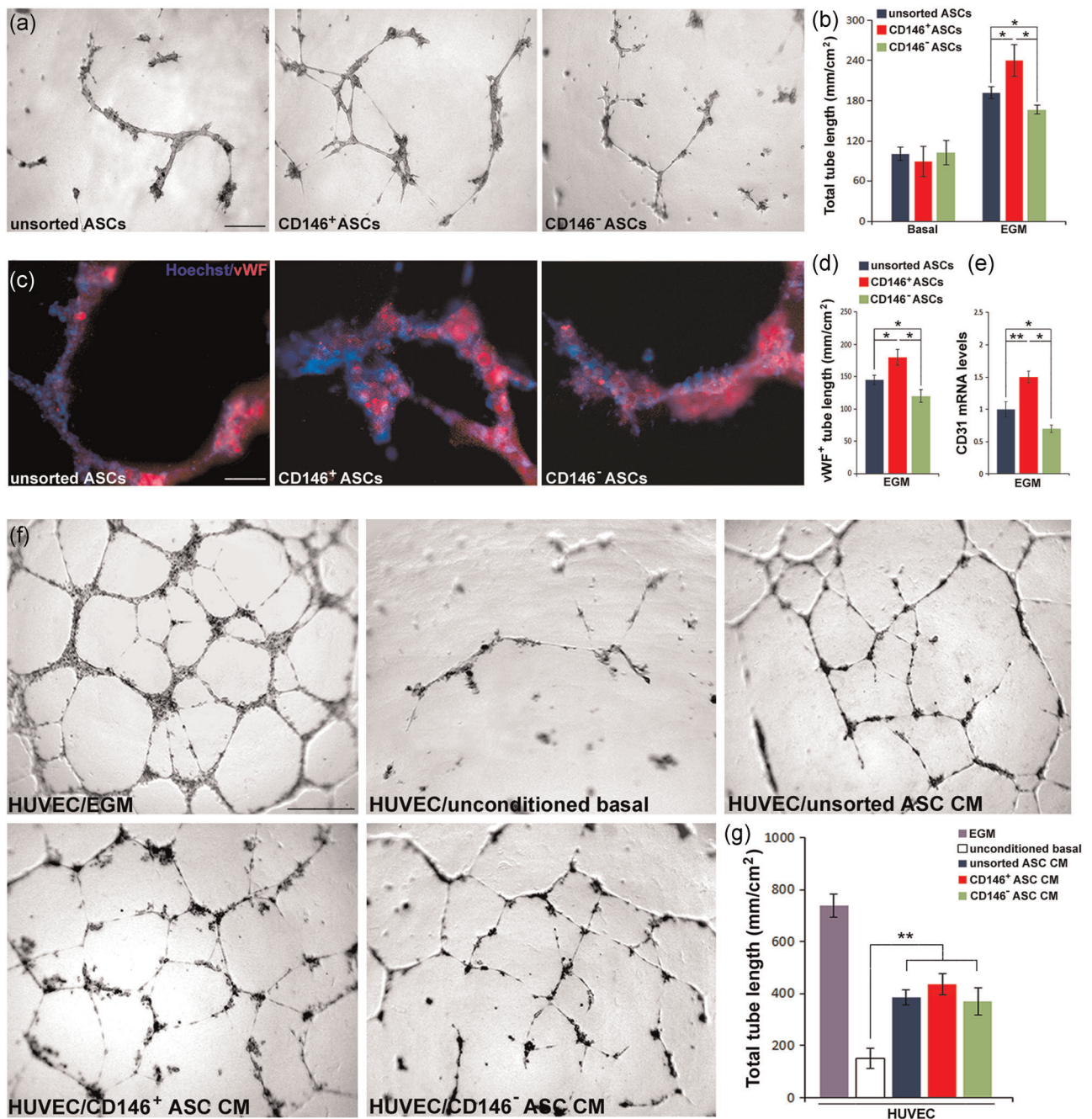


FIGURE 2 Angiogenic potential of human CD146⁺ and CD146⁻ ASCs. (a, b) Tube formation assay of human, unsorted CD146⁺ and CD146⁻ ASCs grown for 72 h in basal medium (DMEM + 10% FBS) or endothelial growth medium (EGM) and then cultured in Matrigel for 24 h (Scale bar = 250 μ m). (c) Capillary-like networks labeled with vWF antibody (red fluorescence; Scale bar = 50 μ m) and (d) morphometric evaluation. (e) Transcript levels of CD31 by real-time PCR. (f, g) Tube formation assay of HUVECs grown with ASC conditioned medium for 72 h and then cultured in Matrigel for 24 h (Scale bar = 250 μ m). EGM and unconditioned basal medium were used as a positive and negative control, respectively. Reported values represent the mean \pm SEM of three independent experiments. ASC, adipose-derived stem cell; DMEM, Dulbecco's modified Eagle's medium; FBS, fetal bovine serum; HUVEC, human umbilical vein endothelial cell; mRNA, messenger RNA; PCR, polymerase chain reaction; vWF, von Willebrand factor. *t*-Test: * $p < .05$ and ** $p < .01$

3.2 | Angiogenic capacity of CD146⁺ is higher than the CD146⁻ ASC subpopulation

As CD146 was considered a pericyte marker, we investigated angiogenic properties of ASCs subpopulations through tube

formation assays and morphometric analysis. Both sorted CD146⁺ and CD146⁻ ASCs were able to form similar capillary networks in the basal medium; however, CD146⁺ displayed a higher angiogenic ability than CD146⁻ and unsorted ASCs in EGM cultures (Figure 2a, b; $p < .05$). The endothelial commitment was confirmed

by vWF staining (Figure 2c,d) and CD31 expression (Figure 2e). The secretion of proangiogenic factors by ASCs was tested via HUVEC tube formation assays. The conditioned medium from unsorted CD146⁺ and CD146⁻ ASCs showed a similar paracrine angiogenic effect on HUVECs, in terms of capillary network development, compared to the unconditioned medium (Figure 2f,g; $p < .01$). The scratch test performed on HUVEC monolayers into the conditioned medium from unsorted CD146⁺ and CD146⁻ ASCs gave similar results; wound closure was greater than into the unconditioned medium (Figure S11a,b; $p < .05$).

3.3 | CD146 expression favored chondrogenesis while its nonexpression favored osteogenesis of sorted ASC subpopulations in 3D collagen scaffolds

We compared the effects of 3D culture systems on the differentiation capabilities of sorted CD146⁺ and CD146⁻ ASCs. Collagen gels were seeded with the ASC subpopulations and cultured in basal and EGM medium for 15 days. CD146⁺ ASC-seeded collagen gels displayed greater contraction than CD146⁻ ASC-seeded ones, more markedly when in the presence of EGM medium (Figure S11a,b; $p < .01$). Microscopic analysis showed differences in structural organization, cell morphology, and extracellular matrix deposition of ASC subpopulations seeded in collagen scaffolds (Figure 3a,b). In particular, Alcian Blue staining (Figure 3c,d) documented a higher GAG accumulation in CD146⁺ ASC-seeded collagen gels, especially in EGM. Quantitative analysis confirmed differences in GAG accumulation (Figure 3g,h; $p < .05$ and $p < .001$, basal and EGM, respectively). Conversely, Alizarin Red staining displayed more calcium deposition in CD146⁻ ASC-seeded collagen scaffolds cultured in basal medium cultures than in CD146⁺ ones (Figure 3e,f). Quantitative analysis of mineralization confirmed these findings (Figure 3g,h; $p < .01$). Chondrogenic (ACAN and COL2A1), osteogenic (ALP and OCN), and endothelial (CD31) markers were in line with histochemical and immunohistochemical findings (Figure 4k,l). In addition, the cartilage hypertrophic markers COL10A1 and MMP13 were not expressed during ASC chondrogenic differentiation. Oil Red O staining for adipogenesis and α -SMA immunoreactivity for myofibroblast differentiation were negative (data not shown).

To confirm the chondrogenic commitment, we analyzed CD146⁺ ASC-seeded collagen scaffolds cultured in EGM by TEM. The ultrastructural examination revealed the presence of cells with a characteristic chondrocyte-like morphology (Figure 4a-d) with abundant cytoplasmic vesicles rich in extracellular matrix content. Extracellular collagen fibers (Figures 4a and 4e,f, arrows) and branched molecules similar to proteoglycan aggregates were also observed (Figures 4b and 4e, arrowheads). The characteristic striation of type II collagen fibers, with a D-period of approximately 60 nm, was also visible at higher magnification (Figure 4e,f). Those findings were similar to those observed in human cartilage controls (Figure 4g-i).

3.4 | CD146⁻ ASCs seeded on HFIP silk scaffolds in basal medium displayed the greatest osteogenic differentiation and mineralization

Differentiation of sorted ASC subpopulations seeded on HFIP silk scaffolds was also investigated. As shown in Figure 5, H&E staining of HFIP silk scaffolds evidenced cell-populated structures (Figure 5a,b). Instead, Alcian Blue staining documented only a slight presence of GAGs in both CD146⁺ and CD146⁻ ASC-seeded HFIP silk scaffolds either in basal or in EGM culture (Figures 5c,d and 5g,h). Alizarin Red staining (Figure 5e,f) and its quantification (Figure 5g,h) evidenced more substantial mineralization in CD146⁻ compared to CD146⁺ ASCs-seeded HFIP silk scaffolds cultured in basal medium ($p < .01$). Osteogenesis disappeared in both CD146⁺ and CD146⁻ ASC-seeded HFIP silk scaffolds in the presence of EGM medium (Figures 5f and 5h), and a weak CD31 positivity was observed (Figure 5i,j). Oil Red O staining and α -SMA immunoreactivity were negative (data not shown). Their negativity supported the absence of adipogenic and myofibroblastic differentiation of ASC subpopulations seeded on HFIP silk scaffolds.

The nature of the mineralization was also investigated by SEM analysis and EDX microanalysis (Figure 6). SEM documented evident modifications even at low magnification. The texture of CD146⁻ ASC-seeded HFIP silk scaffolds appeared more discontinuous and electron-dense than that of empty scaffolds (Figure 6a-d). EDX microanalysis (inserts in Figures 6b and 6d) confirmed the presence of calcium phosphate crystals (hydroxyapatite) close to the clusters of osteoblast-like cells on the surface of the scaffold (Figure 6d, white arrowheads). Those areas rich in adherent osteoblast-like cells resembled the trabecular structure of mouse bone used as control (Figure 6f). No calcium phosphate crystals were detected in the empty scaffold (Figure 6b).

4 | DISCUSSION

In the present study, we documented that CD146 expression has functional implications on osteochondrogenic differentiation of human ASCs. We reported a higher proliferative ability and an increased osteogenic differentiation commitment of sorted CD146⁻ ASCs than unsorted and CD146⁺ ASCs; the latter showed a more significant chondrogenic potential than CD146⁻ and unsorted ASCs in both 2D cultures and 3D collagen scaffolds. These findings demonstrate an evident advantage in terms of differentiation yield in sorted CD146^{+/+}-subpopulations over the unsorted ASCs, although both ASC subpopulations retained the expression of the stromal markers and similar morphology. It has been hypothesized that CD146⁻ adventitial cells can differentiate into pericytes on proper stimulation with a higher proliferative and clonogenic ability, suggesting a perivascular progenitor role (Braun et al., 2013; Corselli et al., 2012; Espagnolle et al., 2014). Zimmerlin et al. (2012, 2010) proposed instead that CD146⁺ pericytes possess a more staminal

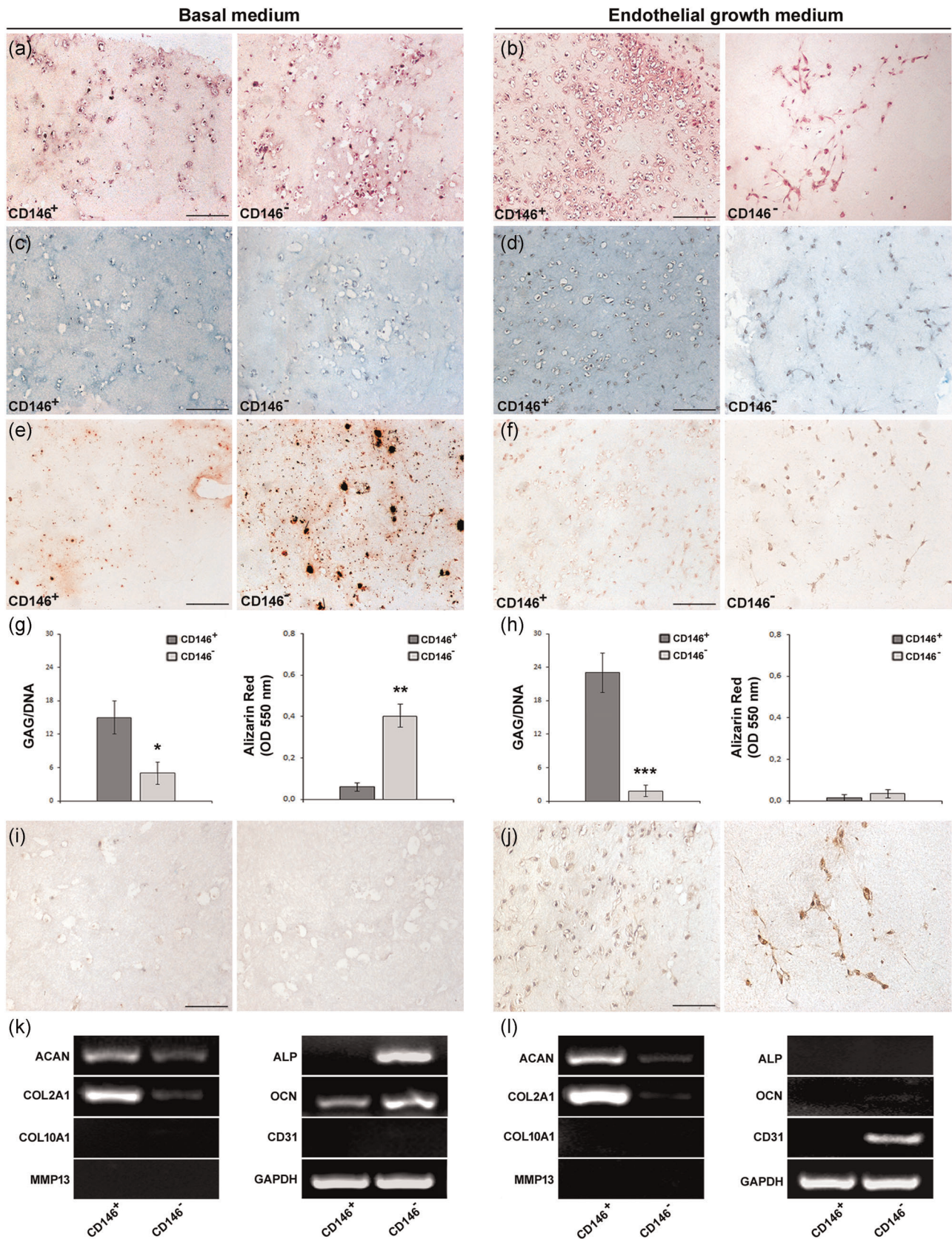


FIGURE 3 (See caption on next page)

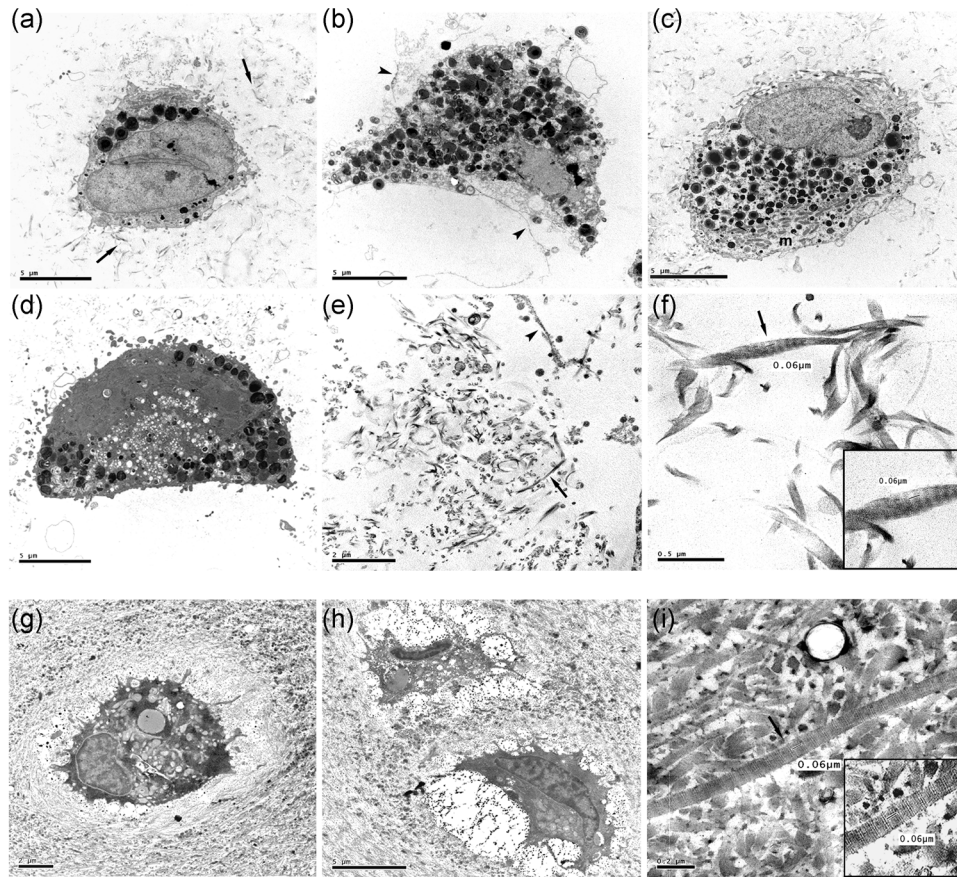


FIGURE 4 Ultrastructural analysis of human CD146⁺ ASCs seeded into collagen gel scaffolds. (a–d) Ultrastructural features of CD146⁺ ASCs seeded into a 3D collagen gel scaffold and cultured with EGM for 15 days. Cells showed a chondrocyte-like morphology with euchromatic nuclei, prominent nucleoli, and abundant mitochondria (m). Moreover, in the cytoplasm are present abundant vesicles containing extracellular matrix rich in fibrils, released in the extracellular space where they self-assembled in collagen fibers (arrows) and branched molecules resembling proteoglycan aggregates (arrowheads). (e) Extracellular matrix consisting of proteoglycan aggregates (arrowhead) and collagen fibers (arrow) showing, at higher magnification, their striation with a λ -period of approximately 60 nm (F plus the inserted detail). (g,h) Control mouse articular cartilage showing chondrocytes embedded in a dense extracellular matrix (I plus the inserted detail) consisting of collagen fibers (arrow) with a λ -period of approximately 60 nm. 3D, three-dimensional; ASC, adipose-derived stem cell; EGM, endothelial growth medium

state with a greater differentiation potential than CD146⁻ adventitial cells. An increased doubling time and senescence of CD146⁻ compared with CD146⁺ ASCs after several passages in culture seems to be in line with that hypothesis (Lauvrud et al., 2017). Nevertheless, we documented that both CD146⁺ and CD146⁻ ASCs retained a vascular commitment, as demonstrated by the tube formation assay and vWF expression in Matrigel. The capacity of

ASCs to develop spontaneously tube-like structures has been previously reported (Madonna & De Caterina, 2008; Natesan et al., 2011; Traktuev et al., 2008). Suga et al. (2009) reported a similar tube formation ability in both pericytes (CD34⁻) and adventitial cells (CD34⁺). In any case, when cultured in EGM, the specific pericyte/endothelial cell medium, the ability of CD146⁺ ASCs to form capillary networks was strongly enhanced compared

FIGURE 3 Osteochondral differentiation of human CD146⁺ ASCs seeded into collagen gel is greater than that of CD146⁻ subpopulation. (a,b) Representative images of H&E stained-sections of human CD146⁺ and CD146⁻ ASCs-seeded collagen gel scaffolds cultured with basal medium or EGM for 15 days (Scale bar = 100 μ m). (c,d) Images of Alcian Blue and (e,f) Alizarin Red staining (Scale bar = 100 μ m). (g,h) Quantification of GAG accumulation and calcium deposits. Reported values represent the mean \pm SEM of three independent experiments performed in triplicate. *t*-Test: **p* < .05, ***p* < .01 and ****p* < .001. (i,j) Representative images of CD31 immunostaining (Scale bar = 50 μ m). (k,l) RT-PCR for chondrogenesis (ACAN, COL2A1), hypertrophy (COL10A1, MMP13), osteogenesis (ALP, OCN), and endothelial (CD31) differentiation markers. ACAN, aggrecan; ALP, alkaline phosphatase; ASC, adipose-derived stem cell; COL2A1, collagen type II alpha 1 chain; COL10A1, collagen X alpha 1 chain; EGM, endothelial growth medium; GAG, glycosaminoglycan; H&E, hematoxylin and eosin; MMP13, matrix metalloproteinase 13; OCN, osteocalcin; OD, optical density; RT-PCR, reverse transcription-polymerase chain reaction

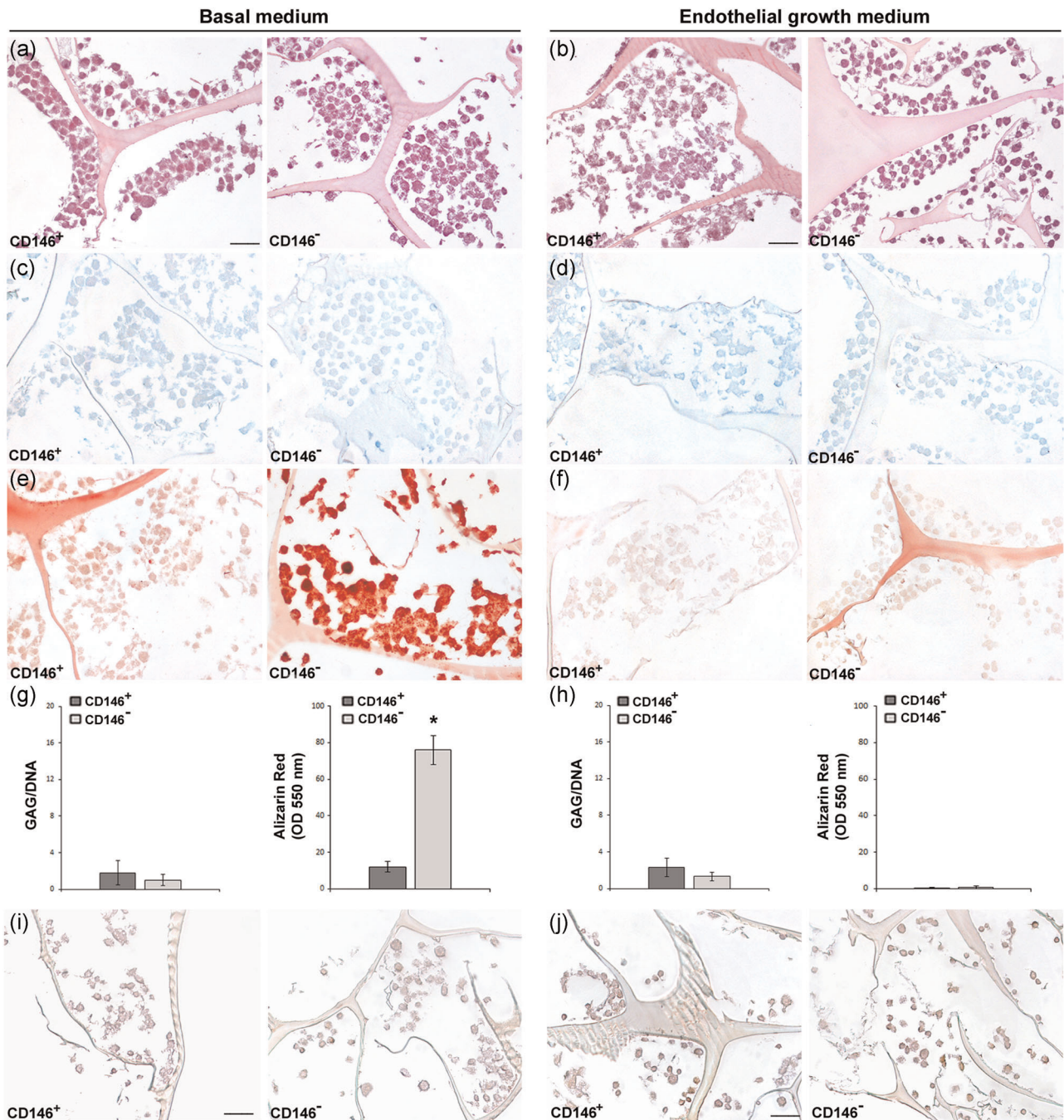


FIGURE 5 Osteogenic differentiation on HFIP silk scaffolds is greater with CD146⁻ ASCs seeding. (a,b) Representative images of H&E stained-sections of human CD146⁺ and CD146⁻ ASCs seeded on HFIP silk scaffolds after 15 days of culture with basal medium or EGM. (c,d) Images of Alcian Blue staining and (e,f) Alizarin Red staining. (g,h) Quantification of GAG accumulation and calcium deposits. (i,j) Representative images of CD31 immunostaining (Scale bar = 50 μ m). Reported values represent the mean \pm SEM of three independent experiments performed in triplicate. ASC, adipose-derived stem cell; EGM, endothelial growth medium; GAG, glycosaminoglycan; H&E, hematoxylin and eosin; HFIP, hexafluoroisopropanol. t-Test: * $p < .01$

to CD146⁻ ASCs. The better differentiative performance of CD146⁺ seems coherent with the hypothesis of a greater stemness (Crisan et al., 2008; Lauvrud et al., 2017; Zimmerlin et al., 2012, 2010) and not due to an autocrine stimulation through increased secretion of proangiogenic factors. In addition, the effects of soluble CD146 on rat placental extravillous trophoblast and endothelial progenitor cells in terms of vascular development,

angiogenesis, and stem cell phenotype maintenance (Essaadi et al., 2018; Kaspi et al., 2013) have been reported. We documented no differences in HUVEC tube formation or proliferation through the scratch test using the conditioned medium from the two ASC subpopulations, suggesting similar autocrine proangiogenic properties. However, apparently conflicting results from the literature reported either a greater expression of endothelial markers in

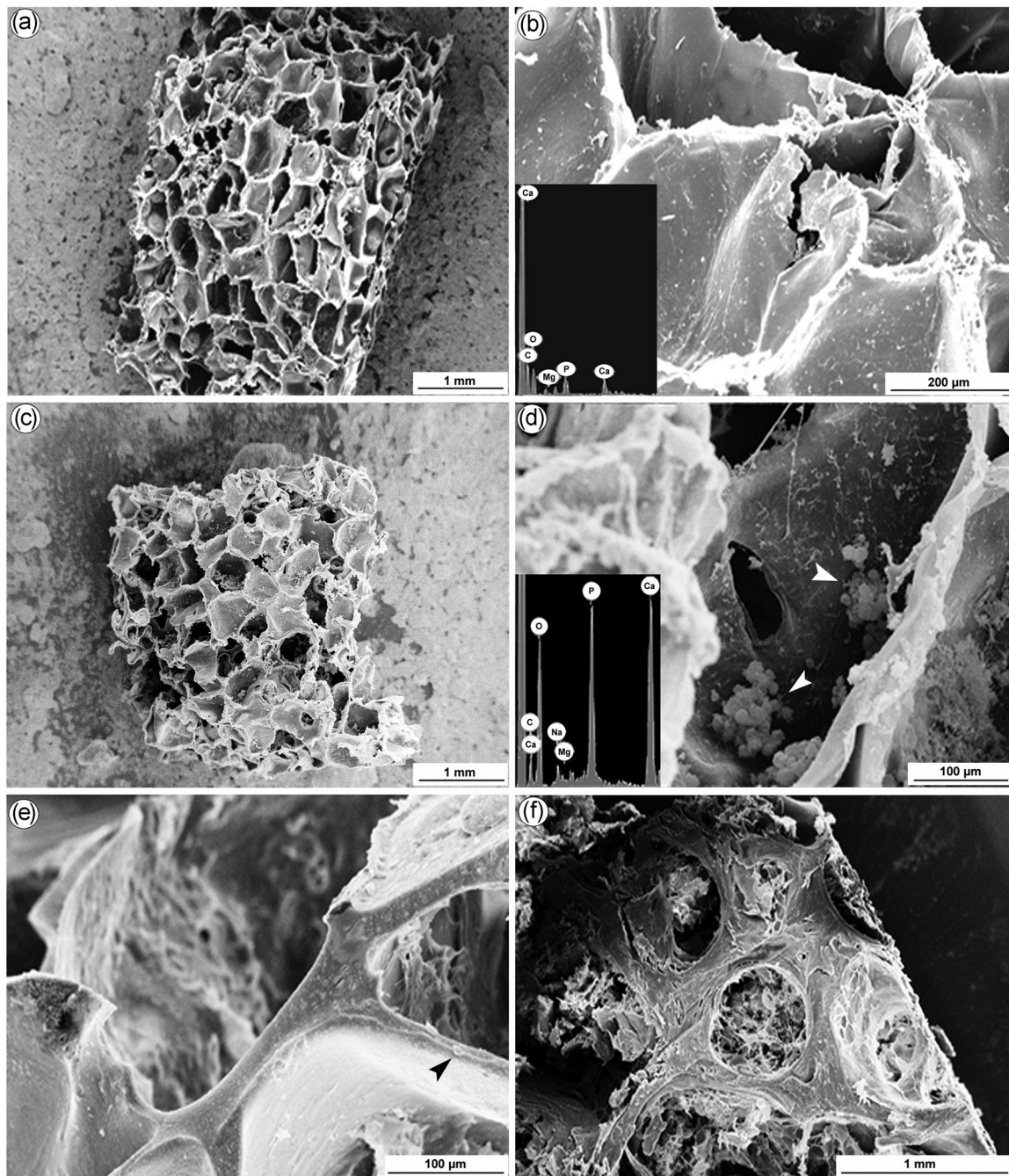


FIGURE 6 Scanning electron microscopy and energy dispersive X-ray microanalysis of CD146⁻ ASCs seeded on HFIP silk scaffold cultured in basal medium. Ultrastructural imaging of the empty scaffold texture (a) with a detail of its surface at higher magnification (b). No osteoblast/osteoblast-like cells and calcium deposits (EDX spectrum, insert in b) are observed. Ultrastructural imaging of the CD146⁻ ASC-seeded scaffold texture (c) and a detail of its surface at higher magnification (d). EDX spectrum (insert in d) showing the presence of hydroxyapatite (calcium phosphate) next to adherent osteoblast/osteoblast-like cells on the scaffold (white arrowheads). (e) Trabecula-like structure in CD146⁻ ASC-seeded HFIP silk scaffold with an osteoblast/osteoblast-like cell on its surface (black arrowhead). (f) Trabecular texture of control mouse spongy bone. ASC, adipose-derived stem cell; EDX, energy dispersive X-ray; HFIP, hexafluoroisopropanol

adventitial cells than in pericytes (Suga et al., 2009) or a differently increased HUVEC capillary formation in CD146⁺ rather than in a CD146⁻ ASC-derived conditioned medium (Lauvrud et al., 2017). Differences may be at least partially explained by differences in experimental protocols.

In a more complex 3D culture model, using both collagen and HFIP silk scaffolds, we documented a noticeable distinct differentiation potential in sorted CD146⁺ and CD146⁻ ASC subpopulations. Collagen is a dense, natural scaffold that provides a biological niche similar to hyaline cartilage (de Mulder et al., 2014). In a basal

medium, CD146⁺ cells embedded into collagen gel showed a spontaneous chondrogenic differentiation, further enhanced by the EGM culture, with no signs of hypertrophy (MMP13 and COL10A1 not expressed). The chondrogenic differentiation in CD146⁺ ASCs embedded into collagen gel was confirmed by the TEM that revealed a chondrocyte-like morphology with the production and secretion of type II collagen fibers in the extracellular space. A correlation between CD146 expression and chondrogenic potential has also been demonstrated in other experiments (Li et al., 2019) as well as in human cartilage-derived and umbilical cord-derived mesenchymal stem cells and in CD146-expressing rat skeletal stem cells (Jiang et al., 2016; Su et al., 2015; Wu et al., 2016). We reported an increased gel contraction in the collagen gel seeded with CD146⁺ ASCs. The gel contraction might represent an indirect sign of chondrogenic differentiation (Nöth et al., 2007) as myofibroblastic differentiation was excluded. The increased chondrogenic differentiation in EGM culture is not a surprise. Apart from proangiogenic factors, EGM contains high concentrations of chondrogenic factors such as ascorbic acid (Temu et al., 2010), IGF-1 (Peng et al., 2019), and heparin (Castilla-Casadiago et al., 2019). Instead, CD146⁻ cells tended to spontaneously form bone in collagen gel under basal medium culture, with limited cartilage production. The propensity of CD146⁻ cells to form bone has also been reported in CD146⁻ bone marrow-derived MSCs (Harkness et al., 2016) and adventitial MSCs during vascular calcification (Xie et al., 2019). However, EGM inhibited osteogenic differentiation of CD146⁻ ASCs, as suggested by the tube-like formation and CD31 positivity. EGM also contains a basic fibroblast growth factor, which has been proven to inhibit osteogenesis and favor chondrogenesis (Kakudo et al., 2007; Quarto et al., 2008). In HFIP silk scaffold culture systems, CD146⁺ cells in the basal medium did not differentiate in cartilage but produced a minimal mineralized matrix deposition. HFIP is a porous, synthetic scaffold with remarkable mechanical properties and has been proven to promote bone more specifically than cartilage formation (Correia et al., 2012). Probably due to its intrinsic characteristics, HFIP scaffolds did not allow chondrogenic differentiation but supported osteogenesis. Scanning electronic microscopy and EDX microanalysis well documented that CD146⁻ ASCs produced abundant matrix, which is calcified in the HFIP structures, like bone trabeculae, by cells themselves. The osteogenic differentiation was inhibited by the addition of EGM, without any reverse chondrogenic commitment, and the outset of a slight angiogenic differentiation in both subpopulations was evident, as showed by the weak CD31 positivity. In conclusion, we documented a functional role of CD146 expression in ASC properties and differentiation commitment without adding exogenous differentiation stimuli, as also observed. The presence in the differentiation media of products unsafe for clinical application constitutes a limitation to their use, thus impairing these models' translational applications. Harnessing the spontaneous differentiation tendency of a discrete ASC subpopulation in suitable culture conditions may support a specific differentiation commitment and represents a promising strategy for future clinical applications in tissue regeneration.

ACKNOWLEDGMENTS

The authors thank Dr. Sabrina Cappelli and Dr. Antonio Volpe for their technical support.

CONFLICT OF INTERESTS

The authors declare that there are no conflict of interests.

AUTHORS CONTRIBUTIONS

Conceptualization, methodology, investigation, writing-original draft preparation: Maria Giovanna Scioli, Gabriele Storti. *Data curation, visualization:* Alessandra Bielli, Massimo Sanchez, Manuel Scimeca. *Supervision, writing-reviewing, editing, and provided funding support:* Jeffrey M. Gimble, Valerio Cervelli, Augusto Orlandi.

ORCID

Augusto Orlandi  <http://orcid.org/0000-0001-7202-5854>

REFERENCES

- Binulal, N. S., Deepthy, M., Selvamurugan, N., Shalumon, K. T., Suja, S., Mony, U., Jayakumar, R., & Nair, S. V. (2010). Role of nanofibrous poly(caprolactone) scaffolds in human mesenchymal stem cell attachment and spreading for *in vitro* bone tissue engineering--response to osteogenic regulators. *Tissue Engineering. Part A*, 16(2), 393-404. <https://doi.org/10.1089/ten.TEA.2009.0242>
- Braun, J., Kurtz, A., Barutcu, N., Bodo, J., Thiel, A., & Dong, J. (2013). Concerted regulation of CD34 and CD105 accompanies mesenchymal stromal cell derivation from human adventitial stromal cell. *Stem Cells and Development*, 22(5), 815-827. <https://doi.org/10.1089/scd.2012.0263>
- Castilla-Casadiago, D. A., García, J. R., García, A. J., & Almodovar, J. (2019). Heparin/collagen coatings improve human mesenchymal stromal cell response to interferon gamma. *ACS Biomaterials Science & Engineering*, 5(6), 2793-2803. <https://doi.org/10.1021/acsbomaterials.9b00008>
- Cervelli, V., Gentile, P., Scioli, M. G., Grimaldi, M., Casciani, C. U., Spagnoli, L. G., & Orlandi, A. (2009). Application of platelet-rich plasma in plastic surgery: Clinical and *in vitro* evaluation. *Tissue Engineering. Part C, Methods*, 15(4), 625-634. <https://doi.org/10.1089/ten.TEC.2008.0518>
- Cervelli, V., Scioli, M. G., Gentile, P., Doldo, E., Bonanno, E., Spagnoli, L. G., & Orlandi, A. (2012). Platelet-rich plasma greatly potentiates insulin-induced adipogenic differentiation of human adipose-derived stem cells through a serine/threonine kinase Akt-dependent mechanism and promotes clinical fat graft maintenance. *Stem Cells Translational Medicine*, 1(3), 206-220. <https://doi.org/10.5966/sctm.2011-0052>
- Cho, S. W., Park, H. J., Ryu, J. H., Kim, S. H., Kim, Y. H., Choi, C. Y., Lee, M. J., Kim, J. S., Jang, I. S., Kim, D. I., & Kim, B. S. (2005). Vascular patches tissue-engineered with autologous bone marrow-derived cells and decellularized tissue matrices. *Biomaterials*, 26(14), 1915-1924. <https://doi.org/10.1016/j.biomaterials.2004.06.018>
- Correia, C., Bhumiratana, S., Yan, L. P., Oliveira, A. L., Gimble, J. M., Rockwood, D., Kaplan, D. L., Sousa, R. A., Reis, R. L., & Vunjak-Novakovic, G. (2012). Development of silk-based scaffolds for tissue engineering of bone from human adipose-derived stem cells. *Acta Biomaterialia*, 8(7), 2483-2492. <https://doi.org/10.1016/j.actbio.2012.03.019>
- Corselli, M., Chen, C. W., Crisan, M., Lazzari, L., & Péault, B. (2010). Perivascular ancestors of adult multipotent stem cells. *Arteriosclerosis, Thrombosis, and Vascular Biology*, 30(6), 1104-1109. <https://doi.org/10.1161/ATVBAHA.109.191643>
- Corselli, M., Chen, C. W., Sun, B., Yap, S., Rubin, J. P., & Péault, B. (2012). The tunica adventitia of human arteries and veins as a source of

- mesenchymal stem cells. *Stem Cells and Development*, 21(8), 1299–1308. <https://doi.org/10.1089/scd.2011.0200>
- Crisan, M., Yap, S., Casteilla, L., Chen, C. W., Corselli, M., Park, T. S., Andriolo, G., Sun, B., Zheng, B., Zhang, L., Norotte, C., Teng, P. N., Traas, J., Schugar, R., Deasy, B. M., Badylak, S., Buhning, H. J., Giacobino, J. P., Lazzari, L., ... Péault, B. (2008). A perivascular origin for mesenchymal stem cells in multiple human organs. *Cell Stem Cell*, 3(3), 301–313.
- Espagnolle, N., Guilloton, F., Deschaseaux, F., Gadelorge, M., Sensébé, L., & Bourin, P. (2014). CD146 expression on mesenchymal stem cells is associated with their vascular smooth muscle commitment. *Journal of Cellular and Molecular Medicine*, 18(1), 104–114. <https://doi.org/10.1111/jcmm.12168>
- Essaadi, A., Nollet, M., Moyon, A., Stalin, J., Simoncini, S., Balasse, L., Bertaud, A., Bachelier, R., Leroyer, A. S., Sarlon, G., Guillet, B., Dignat-George, F., Bardin, N., & Blot-Chabaud, M. (2018). Stem cell properties of peripheral blood endothelial progenitors are stimulated by soluble CD146 via miR-21: Potential use in autologous cell therapy. *Scientific Reports*, 8(1), 9387. <https://doi.org/10.1038/s41598-018-27715-4>
- Frazier, T. P., Bowles, A., Lee, S., Abbott, R., Tucker, H. A., Kaplan, D., Wang, M., Strong, A., Brown, Q., He, J., Bunnell, B. A., & Gimble, J. M. (2016). Serially transplanted nonpericytic CD146(-) adipose stromal/stem cells in silk bioscaffolds regenerate adipose tissue *in vivo*. *Stem Cells*, 34(4), 1097–1111. <https://doi.org/10.1002/stem.2325>
- Gimble, J. M., Katz, A. J., & Bunnell, B. A. (2007). Adipose-derived stem cells for regenerative medicine. *Circulation Research*, 100(9), 1249–1260. <https://doi.org/10.1161/01.RES.0000265074.83288.09>
- Hardy, W. R., Moldovan, N. I., Moldovan, L., Livak, K. J., Datta, K., Goswami, C., Corselli, M., Traktuev, D. O., Murray, I. R., Péault, B., & March, K. (2017). Transcriptional networks in single perivascular cells sorted from human adipose tissue reveal a hierarchy of mesenchymal. *Stem Cells*, 35(5), 1273–1289. <https://doi.org/10.1002/stem.2599>
- Harkness, L., Zaher, W., Ditzel, N., Isa, A., & Kassem, M. (2016). CD146/MCAM defines functionality of human bone marrow stromal stem cell populations. *Stem Cell Research & Therapy*, 7, 4. <https://doi.org/10.1186/s13287-015-0266-z>
- James, A. W., Zara, J. N., Zhang, X., Askarinam, A., Goyal, R., Chiang, M., Yuan, W., Chang, L., Corselli, M., Shen, J., Pang, S., Stoker, D., Wu, B., Ting, K., Péault, B., & Soo, C. (2012). Perivascular stem cells: A prospectively purified mesenchymal stem cell population for bone tissue engineering. *Stem Cells Translational Medicine*, 1(6), 510–519. <https://doi.org/10.5966/sctm.2012-0002>
- Jiang, Y., Cai, Y., Zhang, W., Yin, Z., Hu, C., Tong, T., Lu, P., Zhang, S., Neculai, D., Tuan, R. S., & Ouyang, H. W. (2016). Human cartilage-derived progenitor cells from committed chondrocytes for efficient cartilage repair and regeneration. *Stem Cells Translational Medicine*, 5(6), 733–744. <https://doi.org/10.5966/sctm.2015-0192>
- Joshkon, A., Heim, X., Dubrou, C., Bachelier, R., Traboulsi, W., Stalin, J., Fayyad-Kazan, H., Badran, B., Foucault-Bertaud, A., Leroyer, A. S., Bardin, N., & Blot-Chabaud, M. (2020). Role of CD146 (MCAM) in physiological and pathological angiogenesis-contribution of new antibodies for therapy. *Biomedicine*, 8(12):633. <https://doi.org/10.3390/biomedicine8120633>
- Kakudo, N., Shimotsuma, A., & Kusumoto, K. (2007). Fibroblast growth factor-2 stimulates adipogenic differentiation of human adipose-derived stem cells. *Biochemical and Biophysical Research Communications*, 359(2), 239–244. <https://doi.org/10.1016/j.bbrc.2007.05.070>
- Kang, X., Xie, Y., & Kniss, D. A. (2005). Adipose tissue model using three-dimensional cultivation of preadipocytes seeded onto fibrous polymer scaffolds. *Tissue Engineering*, 11(3-4), 458–468. <https://doi.org/10.1089/ten.2005.11.458>
- Kaspi, E., Guillet, B., Piercecchi-Marti, M. D., Alfaidy, N., Bretelle, F., Bertaud-Foucault, A., Stalin, J., Rabeloson, L., Lacroix, O., Blot-Chabaud, M., Dignat-George, F., & Bardin, N. (2013). Identification of soluble CD146 as a regulator of trophoblast migration: Potential role in placental vascular development. *Angiogenesis*, 16(2), 329–342. <https://doi.org/10.1007/s10456-012-9317-6>
- Lauvrud, A. T., Kelk, P., Wiberg, M., & Kingham, P. J. (2017). Characterization of human adipose tissue-derived stem cells with enhanced angiogenic and adipogenic properties. *Journal of Tissue Engineering and Regenerative Medicine*, 11(9), 2490–2502. <https://doi.org/10.1002/term.2147>
- Li, X., Guo, W., Zha, K., Jing, X., Wang, M., Zhang, Y., Hao, C., Gao, S., Chen, M., Yuan, Z., Wang, Z., Zhang, X., Shen, S., Li, H., Zhang, B., Xian, H., Zhang, Y., Sui, X., Qin, L., ... Guo, Q. (2019). Enrichment of CD146+ adipose-derived stem cells in combination with articular cartilage extracellular matrix scaffold promotes cartilage regeneration. *Theranostics*, 9(17), 5105–5121. <https://doi.org/10.7150/thno.33904>
- Liu, G., David, B. T., Trawczynski, M., & Fessler, R. G. (2020). Advances in pluripotent stem cells: History, mechanisms, technologies, and applications. *Stem Cell Reviews and Reports*, 16(1), 3–32. <https://doi.org/10.1007/s12015-019-09935-x>
- Madonna, R., & De Caterina, R. (2008). *In vitro* neovasculogenic potential of resident adipose tissue precursors. *American Journal of Physiology-Cell Physiology*, 295(5), C1271–C1280. <https://doi.org/10.1152/ajpcell.00186.2008>
- Matsumoto, D., Sato, K., Gonda, K., Takaki, Y., Shigeura, T., Sato, T., Aiba-Kojima, E., Iizuka, F., Inoue, K., Suga, H., & Yoshimura, K. (2006). Cell-assisted lipotransfer: Supportive use of human adipose-derived cells for soft tissue augmentation with lipoinjection. *Tissue Engineering*, 12(12), 3375–3382. <https://doi.org/10.1089/ten.2006.12.3375>
- Mauney, J. R., Nguyen, T., Gillen, K., Kirker-Head, C., Gimble, J. M., & Kaplan, D. L. (2007). Engineering adipose-like tissue *in vitro* and *in vivo* utilizing human bone marrow and adipose-derived mesenchymal stem cells with silk fibroin 3D scaffolds. *Biomaterials*, 28(35), 5280–5290. <https://doi.org/10.1016/j.biomaterials.2007.08.017>
- Merceron, C., Portron, S., Vignes-Colombeix, C., Rederstorff, E., Masson, M., Lesoeur, J., Sourice, S., Siquin, C., Collic-Jouault, S., Weiss, P., Vinatier, C., & Guicheux, J. (2012). Pharmacological modulation of human mesenchymal stem cell chondrogenesis by a chemically oversulfated polysaccharide of marine origin: Potential application to cartilage regenerative medicine. *Stem Cells*, 30(3), 471–480. <https://doi.org/10.1002/stem.1686>
- Mitchell, J. B., McIntosh, K., Zvonic, S., Garrett, S., Floyd, Z. E., Kloster, A., Di Halvorsen, Y., Storms, R. W., Goh, B., Kilroy, G., Wu, X., & Gimble, J. M. (2006). Immunophenotype of human adipose-derived cells: Temporal changes in stromal-associated and stem cell-associated markers. *Stem Cells*, 24(2), 376–385. <https://doi.org/10.1634/stemcells.2005-0234>
- de Mulder, E. L., Hannink, G., van Kuppevelt, T. H., Daamen, W. F., & Buma, P. (2014). Similar hyaline-like cartilage repair of osteochondral defects in rabbits using isotropic and anisotropic collagen scaffolds. *Tissue Engineering. Part A*, 20(3-4), 635–645. <https://doi.org/10.1016/j.jstem.2008.07.003>
- Natesan, S., Zhang, G., Baer, D. G., Walters, T. J., Christy, R. J., & Suggs, L. J. (2011). A bilayer construct controls adipose-derived stem cell differentiation into endothelial cells and pericytes without growth factor stimulation. *Tissue Engineering. Part A*, 17(7-8), 941–953. <https://doi.org/10.1089/ten.TEA.2010.0294>
- Nöth, U., Rackwitz, L., Heymer, A., Weber, M., Baumann, B., Steinert, A., Schütze, N., Jakob, F., & Eulert, J. (2007). Chondrogenic differentiation of human mesenchymal stem cells in collagen type I hydrogels. *Journal of Biomedical Materials Research. Part A*, 83(3), 626–635. <https://doi.org/10.1002/jbm.a.31254>
- Peng, X. B., Zhang, Y., Wang, Y. Q., He, Q., & Yu, Q. (2019). IGF-1 and BMP-7 synergistically stimulate articular cartilage repairing in the

- rabbit knees by improving chondrogenic differentiation of bone-marrow mesenchymal stem cells. *Journal of Cellular Biochemistry*, 120(4), 5570–5582. <https://doi.org/10.1002/jcb.27841>
- Quarto, N., Wan, D. C., & Longaker, M. T. (2008). Molecular mechanisms of FGF-2 inhibitory activity in the osteogenic context of mouse adipose-derived stem cells (mASCs). *Bone*, 42(6), 1040–1052. <https://doi.org/10.1016/j.bone.2008.01.026>
- Scimeca, M., Urbano, N., Bonfiglio, R., Mapelli, S. N., Catapano, C. V., Carbone, G. M., Ciuffa, S., Tavolozza, M., Schillaci, O., Mauriello, A., & Bonanno, E. (2018). Prostate osteoblast-like cells: A reliable prognostic marker of bone metastasis in prostate cancer patients. *Contrast Media & Molecular Imaging*, 2018, 9840962. <https://doi.org/10.1155/2018/9840962>
- Scioli, M. G., Artuso, S., D'Angelo, C., Porru, M., D'Amico, F., Bielli, A., Gentile, P., Cervelli, V., Leonetti, C., & Orlandi, A. (2018). Adipose-derived stem cell-mediated paclitaxel delivery inhibits breast cancer growth. *PLoS One*, 13(9), e0203426. <https://doi.org/10.1371/journal.pone.0203426>
- Scioli, M. G., Bielli, A., Gentile, P., Cervelli, V., & Orlandi, A. (2017). Combined treatment with platelet-rich plasma and insulin favours chondrogenic and osteogenic differentiation of human adipose-derived stem cells in three-dimensional collagen scaffolds. *Journal of Tissue Engineering and Regenerative Medicine*, 11(8), 2398–2410. <https://doi.org/10.1002/term.2139>
- Scioli, M. G., Cervelli, V., Arcuri, G., Gentile, P., Doldo, E., Bielli, A., Bonanno, E., & Orlandi, A. (2014). High insulin-induced down-regulation of Erk-1/IGF-1R/FGFR-1 signaling is required for oxidative stress-mediated apoptosis of adipose-derived stem cells. *Journal of Cellular Physiology*, 229(12), 2077–2087. <https://doi.org/10.1002/jcp.24667>
- Stasi, M. A., Scioli, M. G., Arcuri, G., Mattered, G. G., Lombardo, K., Marcellini, M., Riccioni, T., De Falco, S., Pisano, C., Spagnoli, L. G., Borsini, F., & Orlandi, A. (2010). Propionyl-L-carnitine improves postischemic blood flow recovery and arteriogenic revascularization and reduces endothelial NADPH-oxidase 4-mediated superoxide production. *Arteriosclerosis, Thrombosis, and Vascular Biology*, 30(3), 426–435. <https://doi.org/10.1161/ATVBAHA.109.201533>
- Su, X., Zuo, W., Wu, Z., Chen, J., Wu, N., Ma, P., Xia, Z., Jiang, C., Ye, Z., Liu, S., Liu, J., Zhou, G., Wan, C., & Qiu, G. (2015). CD146 as a new marker for an increased chondroprogenitor cell sub-population in the later stages of osteoarthritis. *Journal of Orthopaedic Research*, 33(1), 84–91. <https://doi.org/10.1002/jor.22731>
- Suga, H., Matsumoto, D., Eto, H., Inoue, K., Aoi, N., Kato, H., Araki, J., & Yoshimura, K. (2009). Functional implications of CD34 expression in human adipose-derived stem/progenitor cells. *Stem Cells and Development*, 18(8), 1201–1210. <https://doi.org/10.1089/scd.2009.0003>
- Temu, T. M., Wu, K. Y., Gruppuso, P. A., & Phornphutkul, C. (2010). The mechanism of ascorbic acid-induced differentiation of ATDC5 chondrogenic cells. *American Journal of Physiology-Endocrinology and Metabolism*, 299(2), E325–E334. <https://doi.org/10.1152/ajpendo.00145.2010>
- Traktuev, D. O., Merfeld-Clauss, S., Li, J., Kolonin, M., Arap, W., Pasqualini, R., Johnstone, B. H., & March, K. L. (2008). A population of multipotent CD34-positive adipose stromal cells share pericyte and mesenchymal surface markers, reside in a periendothelial location, and stabilize endothelial networks. *Circulation Research*, 102(1), 77–85. <https://doi.org/10.1161/CIRCRESAHA.107.159475>
- Wu, J., Sun, Y., Block, T. J., Marinkovic, M., Zhang, Z. L., Chen, R., Yin, Y., Song, J., Dean, D. D., Lu, Z., & Chen, X. D. (2016). Umbilical cord blood-derived non-hematopoietic stem cells retrieved and expanded on bone marrow-derived extracellular matrix display pluripotent characteristics. *Stem Cell Research & Therapy*, 7(1), 176. <https://doi.org/10.1186/s13287-016-0437-6>
- Xie, C., Ouyang, L., Chen, J., Zhang, H., Luo, P., Wang, J., & Huang, H. (2019). The emerging role of mesenchymal stem cells in vascular calcification. *Stem Cells International*, 2019, 2875189. <https://doi.org/10.1155/2019/2875189>
- Zannettino, A. C., Paton, S., Arthur, A., Khor, F., Itescu, S., Gimble, J. M., & Gronthos, S. (2008). Multipotential human adipose-derived stromal stem cells exhibit a perivascular phenotype *in vitro* and *in vivo*. *Journal of Cellular Physiology*, 14(2), 413–421. <https://doi.org/10.1002/jcp.21210>
- Zimmerlin, L., Donnenberg, V. S., & Donnenberg, A. D. (2012). Pericytes: A universal adult tissue stem cell? *Cytometry. Part A: The Journal of the International Society for Analytical Cytology*, 81(1), 12–14. <https://doi.org/10.1002/cyto.a.21168>
- Zimmerlin, L., Donnenberg, V. S., Pfeifer, M. E., Meyer, E. M., Péault, B., Rubin, J. P., & Donnenberg, A. D. (2010). Stromal vascular progenitors in adult human adipose tissue. *Cytometry. Part A: The Journal of the International Society for Analytical Cytology*, 77(1), 22–30. <https://doi.org/10.1002/cyto.a.20813>
- Zuk, P. A., Zhu, M., Ashjian, P., De Ugarte, D. A., Huang, J. I., Mizuno, H., Alfonso, Z. C., Fraser, J. K., Benhaim, P., & Hedrick, M. H. (2002). Human adipose tissue is a source of multipotent stem cells. *Molecular Biology of the Cell*, 13(12), 4279–4295. <https://doi.org/10.1091/mbc.e02-02-0105>

SUPPORTING INFORMATION

Additional Supporting Information may be found online in the supporting information tab for this article.

How to cite this article: Scioli, M. G., Storti, G., Bielli, A., Sanchez, M., Scimeca, M., Gimble, J. M., Cervelli, V., & Orlandi, A. (2021). CD146 expression regulates osteochondrogenic differentiation of human adipose-derived stem cells. *Journal of Cellular Physiology*, 1–14. <https://doi.org/10.1002/jcp.30506>